Role of boron on the Spark Plasma Sintering of an α-SiC powder

A. Maitrerobert, Aurélie Vande Put, Jean-Paul Laval, Stéphane Valette, Gilles Trolliard

Role of boron on the Spark Plasma Sintering of an α-SiC powder

A. Maître *, A. Vande Put, J.P. Laval, S. Valette, G. Trolliard

Laboratoire Science des Procédés Céramiques et Traitements de Surface, UMR CNRS 6638, 123, Avenue Albert Thomas, F-87060 LIMOGES Cedex, France

Abstract

This study deals with the role of non-oxide sintering aids such as boron carbide (B_4C) or – free boron (B) plus free carbon (C) – on the Spark Plasma Sintering treatment of silicon carbide. The results so obtained clearly show that free boron plus free carbon additions lead to the higher densification rates. This favourable behaviour with regards to the densification kinetics is accompanied by the absence of any abnormal grain growth. At the opposite, boron carbide additions do not significantly raise the densification kinetic after SPS treatment of SiC in comparison to pure silicon carbide. In this case, TEM investigations point out the formation of a borosilicate vitreous phase due to the dissolution process of B_4C in contact with a native superficial silica layer surrounding the SiC grains. The resulting liquid phase leads to an abnormal grain growth coupled with undensifying process.

Keywords: SiC; SPS; Sintering; Grain growth; Boron; Carbon

1. Introduction

Silicon carbide (SiC) is a very interesting ceramic due to its promising properties like high hardness, low bulk density, high oxidation resistance which makes it useful for a wide range of industrial applications (nuclear fuels coating for future reactors, thermal barrier for aeronautic or aerospace applications). In addition to the interest in its properties for structural applications, silicon carbide has also been the focus of investigations for its chemical resistance in cryolithic melts.[1] It has more particularly received considerable attention as sidelining material in aluminum electrolysis cells.[2]

Unfortunately, like so many other covalent refractory ceramics, the silicon carbide is very difficult to sinter to a high density without using additives and/or pressure. For example, without any additives, the theoretical density could only be achieved at 2500 °C by hot-pressing under a pressure of 50 MPa.[3]

In previous studies, it is shown that using sintering aids could lower the sintering temperature. Several additives like YAG (*i.e.* the $Y_3Al_5O_{12}$ compound) and alumina were tested as sintering aids for silicon carbide powder both to enhance the densification rate and to slow down grain growth kinetic.[4,5] The sintering mechanism was determined for each of these additives considered separately and in the case of alumina, supplement adding of carbon or yttria were also performed. In these conditions, it is worth to notice that alumina together with carbon promoted silicon carbide sintering via solid-state sintering at temperature over 2000 °C[4] while alumina and yttria led to high density sintered sample via liquid phase sintering below 2000 °C.[5]

In these approaches where additives are mainly oxides, the consolidation steps principally take place through liquid phase sintering,[5] giving rise to the formation of an interphase at the grain boundaries. In contact with melted salts, the so-formed secondary phases show lower corrosion resistance than the SiC matrix.[1,2] To achieve high densities through solid-state sintering and to avoid the appearance of low corrosion resistance intergranular phases, consolidation of silicon carbide with boron and carbon as sintering additives seems to be the most efficient way.[6–9] Therefore, boron carbide was found to enhance the hot-pressing behaviour of silicon carbide that could be so obtained in a fully dense state.[10–12] These additives permit to reach high density slightly over 2000 °C by means of the reduction of the surface energy of the grains (boron effect)[10] and reaction with residual silica (carbon effect).[11]

* Corresponding author. Tel.: +33 5 55 45 74 63; fax: +33 5 55 45 75 86.
E-mail address: alexandre.maitre@unilim.fr (A. Maître).

doi:10.1016/j.jeurceramsoc.2008.01.002

Otherwise, several contributions[13,14] were devoted to the consolidation of silicon carbide powders to produce dense bodies by using Spark Plasma (or pulse electric current) Sintering (SPS). In all these studies, the main goal is to avoid or to minimize the grain growth of the starting SiC nanoparticles. Indeed, it is usually well admitted that grain growth can be suppressed during the SPS treatment of ceramics because of the very short sintering time.[15–17] However, Zhou et al.[18] revealed that the rapid densification of a nanometer sized β-SiC powder doped with 2.04 wt% Al_4C_3 and 0.4 wt% B_4C and conducted by SPS technique, was accompanied by significant microstructural and structural evolutions. Indeed, the densified SiC specimens underwent anisotropic grain growth and polytype transformation. According to these authors,[19] the $\beta \rightarrow \alpha$ transformation during SPS would contribute both to the anisotropic grain growth of SiC (*i.e.* the formation of elongated grains) and to the modifications of the amount of the different polytypes. In the same manner, the SPS conditions (*e.g.* the heating rate) could strongly influence the $\beta \rightarrow \alpha$ transformation. Unfortunately, the role of the sintering additives, especially boron carbide, was not considered to explain this significant microstructural evolution of SiC-based samples.

In the present study, the SPS method was used to produce fully dense SiC-based materials with non-oxide secondary phases in order to provide high corrosion resistance sidelining materials for Al electrolysis cells. The second objective was to focus on the role of boron during the Spark Plasma Sintering of a commercial α-silicon carbide powder. The structural and microstructural evolutions due to different boron additions (free boron plus free carbon or boron carbide (B_4C)) were characterized by transmission electron microscopy (TEM) and Fourrier transform infra-red (FTIR) spectrometry techniques.

2. Experimental procedure

2.1. Starting powders

The main physical-chemistry properties of raw materials (specific area, average grain size, purity) were summarized in Table 1.

α-Silicon carbide powder supplied by H.C. Starck™ (grade UF 25) was used as starting powder. From its X-ray diffraction pattern (Fig. 1), it can be noticed that this silicon carbide powder mainly contains 6H and 4H polytypes (JCPDS files 72-0018 and 29–1127, respectively).

Sintering additives provided by H.C. Starck™, Prolabo™ and Cerac™ suppliers (Table 1) were added under several forms.

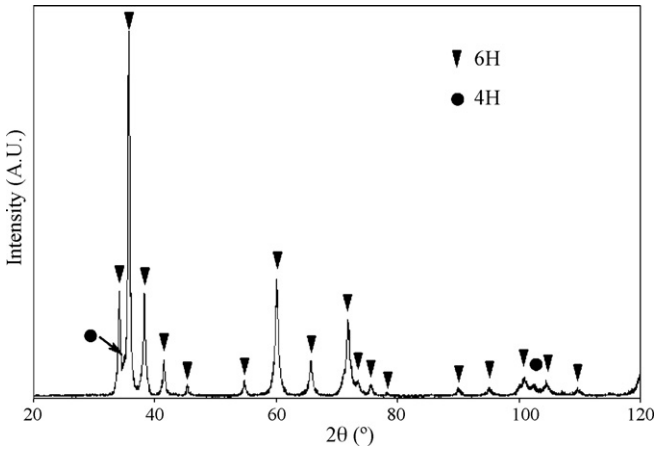

Fig. 1. X-ray diffraction pattern of the starting silicon carbide powder.

When amorphous boron and carbon were introduced in the mixture as free elements, their respective amount was 3.1 wt% and 0.86 wt%, *i.e.* the same weight ratio as for B_4C. Different symbols have been used in the present paper to make the sample description easier:

- "SBC" indicates samples in which both free boron and free carbon have been added to the starting silicon carbide powder;
- "SB4C" stands for samples in which boron carbide additions are introduced in the same SiC powder.

Scanning electron microscopy (SEM) observations of silicon carbide powder are reported in Fig. 2. The powder consists in agglomerates of a few micrometers (Fig. 2a) which are formed of elementary particles of few hundred nanometres in size (Fig. 2b). Fig. 3 represents the microstructures of the sintering agent powders. Both free carbon and boron (Fig. 3a and b, respectively) are mainly composed of agglomerated equiaxed particles while B_4C displays micron size angular platelet microstructure (Fig. 3c).

2.2. Sample preparation and sintering procedure

α-SiC and sintering aids were mixed in petroleum ether (Riedel de Häen, "extra pure" quality) according to the chosen proportions and then dispersed by ultrasonic pulses. The mix was dried under vacuum at 80 °C in order to remove the solvent.

For SPS treatments, the powders were then put in a 15 mm diameter graphite die in which some thin papyex™ graphite foils were fetched on the inner surface. The sintering of SiC powder with or without sintering additives was conducted under vacuum ($6 < P(\text{Pa}) < 14$). The SPS apparatus (Model 2080 Sum-

Table 1
Main physical-chemistry of the starting powders

Powder (supplier)	Variety	Specific area (m^2/g)	Mean diameter[a] (μm)	Purity (%)
Silicon carbide (H.C. Starck)	α-SiC (6H, 4H)	26.70	0.07	98
Boron carbide (H.C. Starck)	B_4C	17.77	0.13	97
Boron (Cerac)	Amorphous	16.05	0.16	99.9
Carbon (Prolabo)	Lampblack	25.70	0.25	Ashes < 0.75

[a] The mean equivalent diameter $\emptyset$ is calculated on the basis of the density ρ and of the measured specific area S by the classical relation: $\emptyset = 6/(\rho \times S)$.

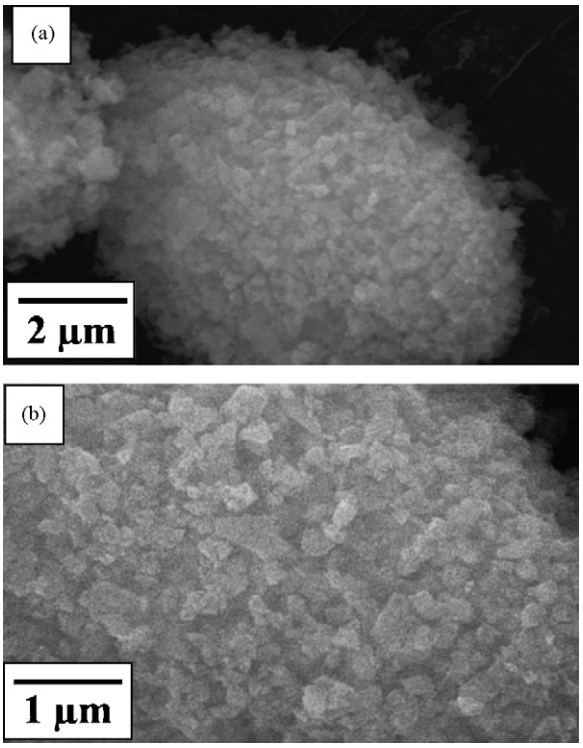

Fig. 2. SEM observations of the starting silicon carbide powder at different magnifications.

itomo Coal and Mining Co.) is a uniaxial 100 kN press combined with a 8000 A dc power supply to provide simultaneously pulsed current and pressure to the sample. The standard 12:2 pulse sequence[19] which corresponds to 12 dc current pulses and two pulses off was chosen. The SPS thermal treatment was as following:

- A degassing treatment performed at 600 °C during 5 min: 3 min under limited applied load (20 MPa) and 2 min under increasing load up to 40 MPa or 100 MPa.
- A heating up to 1850 °C or 1950 °C at 100 °C min^{-1} under optimal applied load (40 MPa or 100 MPa), a soaking time of 5 min at maximum temperature then cooling down to room temperature.

The experimental parameters such as temperature, applied load, voltage and sample displacement were measured continuously during the sintering treatment. In particular, the temperature was measured thanks to a digital pyrometer focused on the graphite die close to the centre of the sample.

2.3. Characterization of sintered samples

The phase identification was performed using a X-ray Siemens D5000 diffractometer ($\lambda_{Cu} = 0.1541$ nm) equipped with a back monochromator. The scanned angles (in 2θ scale) were ranging between 15° and 120° with a step of 0.02° and a 13 s exposure time. The X-ray diffractograms were indexed using the DIFFRAC+ software (Socabim) which contained JCPDS files data base. Accurate measurements of the relative abundance of the various polytypes present in silicon carbide based samples were carried out using the Rietveld's method implemented into the TOPAS 3 program.[20] The X-ray patterns were acquired from sintered samples previously ball milled in an agate mortar under cryogenic conditions.

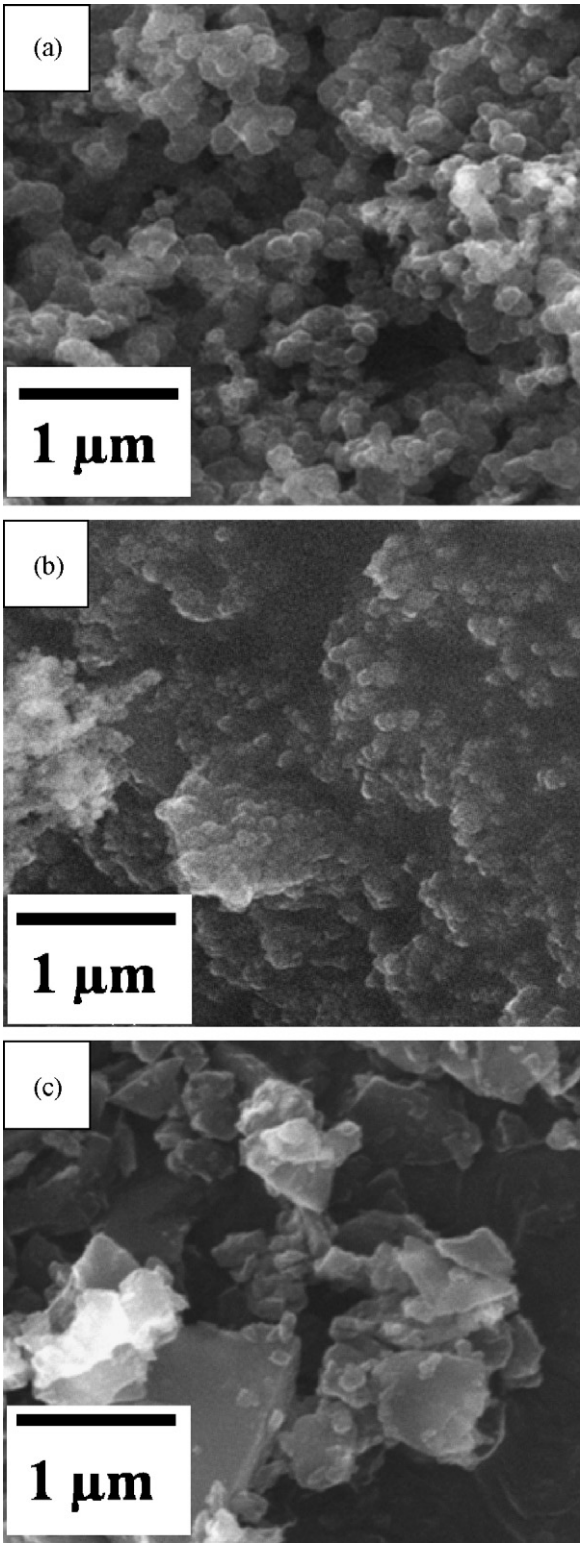

Fig. 3. SEM observations of the starting powders: carbon lampblack (a), boron (b) and boron carbide: B_4C (c).

The infrared spectroscopic measurements (FTIR) were carried out using a PerkinElmer Spectrum 1000 apparatus. The spectra were registered in the 400–4000 cm^{-1} range with a 2 cm^{-1} resolution. FTIR measurements were performed from starting powders and sintered samples which were previously ball milled.

Density of sintered samples was determined using Archimedes method. The microstructural analyses were carried out using SEM Philips XL30 apparatus. The identification of the intergranular phases required TEM investigations which were performed with a 2010 JEOL apparatus equipped with EDX facilities (Energy Dispersive X-ray analytical system) and operating at 200 kV. As such, specimens were prepared by cutting samples into thin disks with a 3 mm diameter. These disks were ground, dimpled and finally thinned to perforation by argon beam milling in a Gatan Precision Ion Polishing System (PIPS 692) at 4 kV.

3. Results

3.1. Densification kinetics

Fig. 4a shows the variation of the linear shrinkage for SiC-based samples doped with different sintering aids under a 100 MPa applied load as a function of temperature during the SPS treatment. From this figure, it can be noticed that the densification of SiC samples starts at lower temperatures when boron-based sintering additives are initially introduced. The temperature of the shrinkage beginning (T_S) is reported in Fig. 4b. T_S values were determined using a polynomial interpolation in order to fit the curves showing the linear shrinkage (Fig. 4a) and then to determine the continuous variation of $d(\Delta L)/dT$ as a function of temperature. For a given sample, the T_S value is thus defined as the temperature where $d(\Delta L)/dT$ deviates from the straight line in the low temperature range. The data so obtained were reported in Fig. 4b. From the latter, the temperature of the shrinkage beginning seems to be shifted towards lower temperatures by using sintering aids for the same applied load. For example, in the case of SBC, the T_S value (*i.e.* ≈1200 °C) was 220 °C lower than that recorded for pure silicon carbide specimens under an 40 MPa applied load (see Fig. 4b).

Moreover, the higher the applied load during SPS treatment, the higher the densification kinetics whatever the sintering aids. In particular, the lowest temperature of the shrinkage beginning was reached (*i.e.* 1190 °C) when a 100 MPa load was applied during the treatment of SBC samples.

Table 2 provides the relative density for specimens treated by SPS at 1850 °C or 1950 °C for 5 min under a 40 MPa or 100 MPa load. The treatments at 1950 °C under 100 MPa gave relative density values higher than 97.5% regardless the sintering additive. This fact is confirmed by the observation of the sintering curves under isothermal conditions which denotes that fully dense materials are obtained at 1950 °C for a soak time fixed to 5 min (see Fig. 4c). Therefore, the theoretical density of SiC-based specimens was achieved when the maximum load was applied and the SBC composition was retained (Table 2).

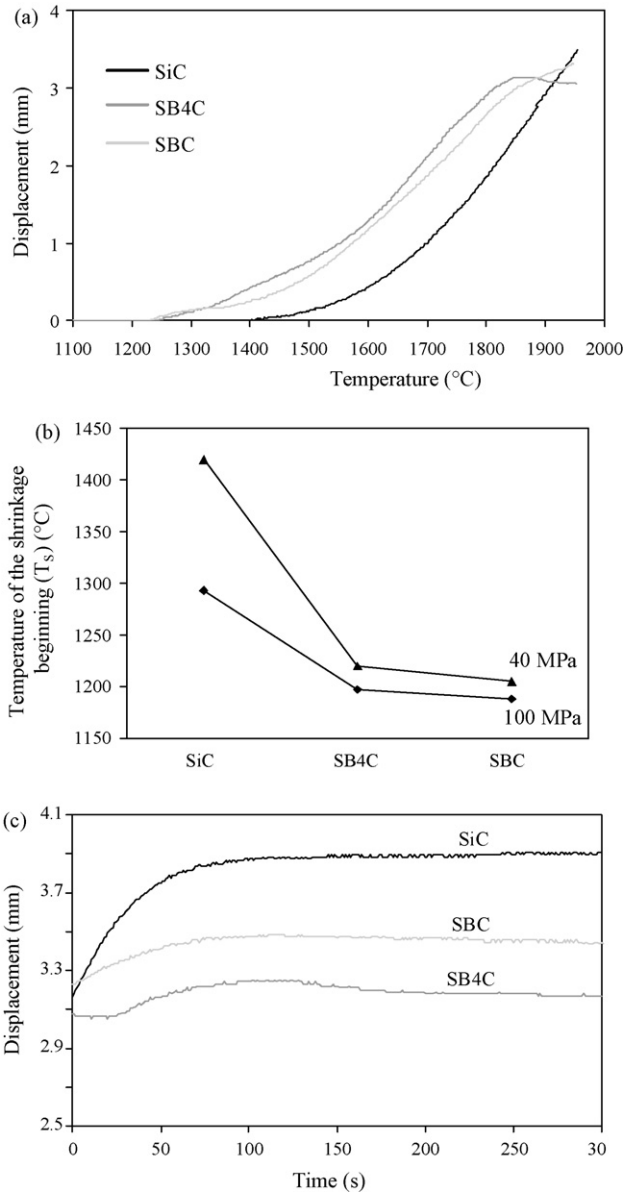

Fig. 4. Sintering curves as a function of temperature under a 100 MPa applied load for pure SiC, SBC and SB4C samples (heating rate = 100 °C min^{-1}) (a). Temperature of shrinkage beginning (T_S) determined for the different SiC-based samples obtained by Spark Plasma Sintering (SPS) treatments under different applied loads (b). Densification curves as a function of soaking time under isothermal conditions (at 1950 °C) and a 100 MPa applied load for pure SiC, SBC and SB4C samples (c).

In the following and due to their high densification rates, the materials sintered for 5 min at 1950 °C under a 100 MPa load will be characterized by TEM, XRD and FTIR techniques.

3.2. Characterization of the different silicon carbide polytypes

X-ray diffraction patterns obtained from pure SiC, SBC and SB4C samples treated at 1950 °C for 5 min under 100 MPa have been reported in Fig. 5. Compared to the SiC starting powder (Fig. 1), all sintered samples are characterized by the occurrence of the 15R rhombohedral form (identified from JCPDS

Table 2
Sintering conditions, relative density and polytype content of the SPS-sintered SiC ceramics

Silicon carbide	Sintering temperature (°C)	Heating rate (°C min^{-1})	Holding time (min)	Load (MPa)	Relative density (%)	Weight percentage of silicon carbide polytypes		
						6H	4H	15 R
Pure SiC	1950	100	5	100	97.5	88.35	4.95	6.70
	1850	40	5	40	92.8	–	–	–
SBC sample (SiC + free boron + free carbon)	1950	100	5	100	98.8	88.60	5.66	5.84
	1850	40	5	40	93.7	–	–	–
SB4C sample (SiC + boron carbide)	1950	100	5	100	97.1	84.59	11.29	4.12
	1850	40	5	40	91.9	–	–	–

file 39-1196 reported in Fig. 5b) in addition to the 6H and 4H polytypes. To quantify the respective amount of the three polytypes, a simultaneous refinement of the three structures was performed, using the TOPAS 3 Rietveld program.[20] Indeed, previous works demonstrated that the Rietveld's method yielded accurate phase composition measurements within a maximum 1 wt%.[21] The reference structures were taken from the ICSD database.[22] Then, the structures were partly refined (scale factors and isotropic thermal vibration factors) keeping the atomic positions unchanged. After convergence to reasonable *R* factor values, the quantitative fraction of the three polytypes was determined with a good accuracy and the corresponding data is shown in Table 2. It is shown that the 15R polytype occurs in a significant amount even if the 6H and 4H polytypes remain predominant. Moreover, the 4H polytype amount in sintered samples seems to be particularly great for SB4C samples in comparison with that registered for "pure" SiC or SBC specimens (see Table 2) after SPS.

3.3. Microstructural study of the sintered samples

3.3.1. Pure silicon carbide

TEM observations of pure SiC samples revealed the presence of an equiaxed microstructure (Fig. 6a). No preferential crystalline orientation was observed. The grain size averages

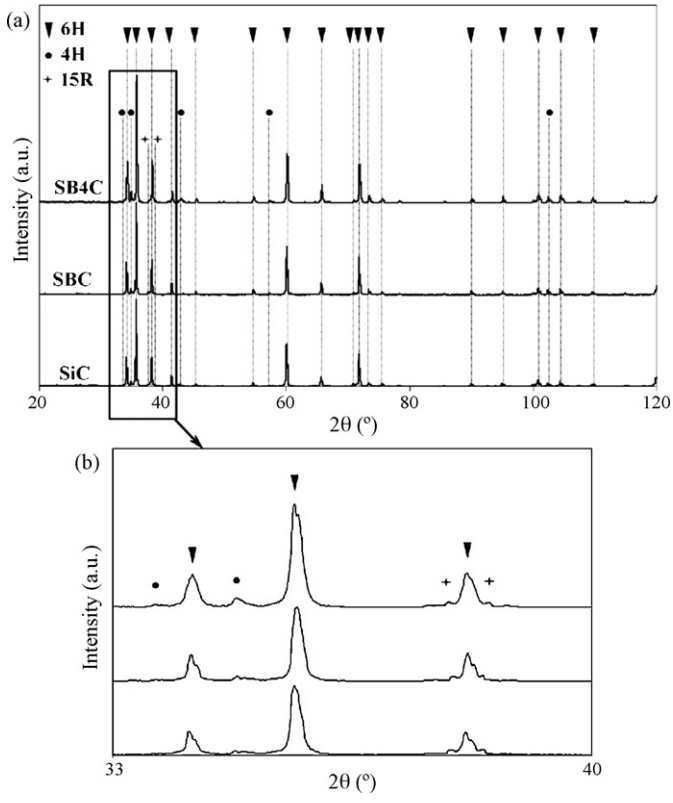

Fig. 5. X-ray diffraction patterns obtained on the samples sintered by SPS (1950 °C for 5 min under a 100 MPa pressure): pure SiC samples (SiC), SiC samples plus free boron and carbon addings (SBC), SiC samples plus boron carbide addings (SB4C) (a). Enlargement of the framed area in (a) showing the diffraction peaks of the different SiC polytypes (b).

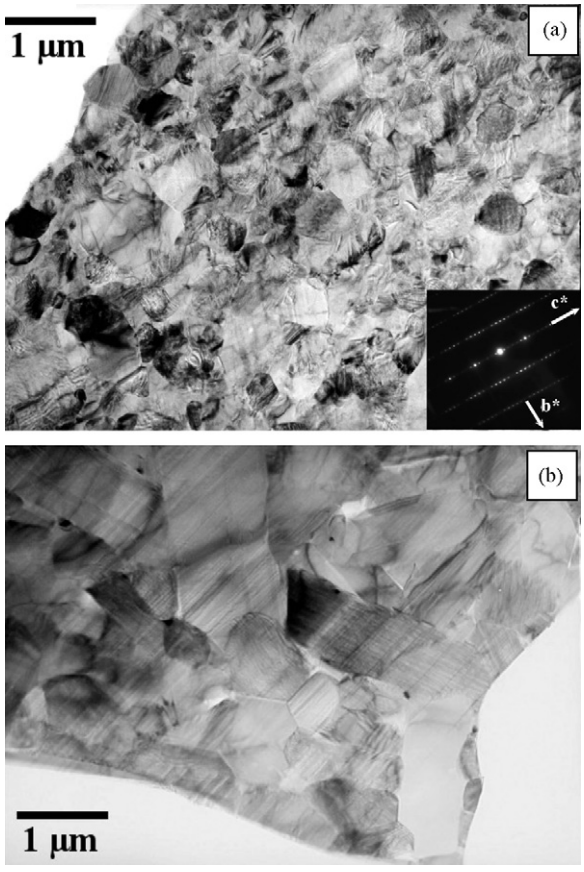

Fig. 6. TEM micrographs obtained on the samples sintered by SPS (1950 °C for 5 min under a 100 MPa pressure): pure SiC samples (a), SiC samples with free boron and carbon as sintering aids (SBC) (b).

500 nm and remains quite the same as that of the starting powder (see Fig. 2b). The electron diffraction study confirmed that the 6H polytype is the main phase presents within the sample (see inset in Fig. 6a).

3.3.2. SBC samples

A change in microstructure occurred when free boron and free carbon were added to the starting SiC powder (Fig. 6b). A heterogeneous grain size is observed contrasting with the microstructure of SiC samples presented above. Some of the grains have preferentially grown, showing elongated shape while most of them kept the equiaxed shape. No intergranular thin film of secondary phase linked to free boron and free carbon addings was detected either by conventional contrast imaging or by high resolution investigation of grain boundaries. These results however do not definitely preclude the possibility of atomic segregation of species at the grain boundaries as will be further discussed.

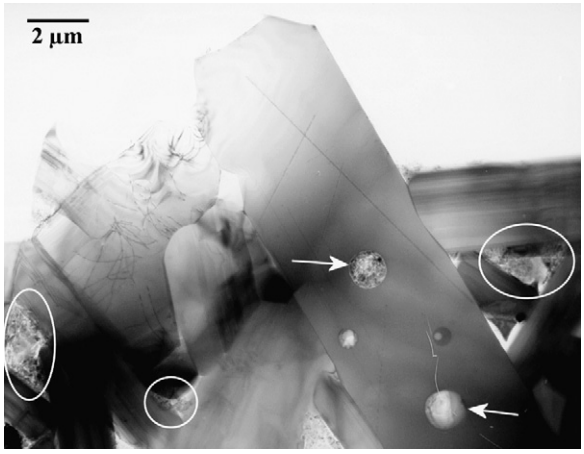

Fig. 7. TEM micrograph of a SiC samples after SPS at 1950 °C for 5 min under 100 MPa with boron carbide addings (SB4C). The lath-type microstructure accounts for abnormal grain growth. The presence of an intergranular phase at triple junctions (encircled areas) and of intragranular inclusions (see arrows) is noticeable.

3.3.3. SB4C samples

Observations of SB4C sintered samples (Fig. 7) showed up microstructural changes compared to pure SiC and SBC samples presented above. The microstructure was characterized by abnormal grain growth with lath-type texture linked to the anisotropic character of the SiC polytypes. This grain growth was accompanied by a slight undensifying effect as shown by the results reported in Table 2.

The sample typically presents numerous spherical intragranular inclusions (Fig. 7: see arrows) as well as intergranular phase (Fig. 7: encircled areas) trapped between lath shaped SiC crystals and B_4C crystals (Fig. 8a).

In fact, the intergranular phases are present in reactional zones involving B_4C crystals. Indeed, the latter are highly corroded as shown by the presence of numerous corrosion gulfs all around the crystals (Fig. 8a: see arrows). In most cases, such crystals of parent phase are entirely dissoluted and relicts of the boron carbide crystals are only seldom seen. For that reason, this residual phase is not observed in XRD patterns presented in Fig. 5. When exist, the intergranular phase around the B_4C crystals (Fig. 8a, c and d) consists of nanocrystals of about 50 nm embedded within an amorphous phase. An average chemical analysis performed with a defocused electron beam reveals that this phase is made of carbon, silicon and oxygen (Fig. 8b). A fine investigation of this area (Fig. 9) shows that the amorphous phase is mainly composed of a silicon oxide (Fig. 9b) while nanocrystals are composed of carbon (Fig. 9a) that could be present under graphite or diamond forms. The investigation of their reciprocal lattice by electron diffraction attests of a cubic structure and,

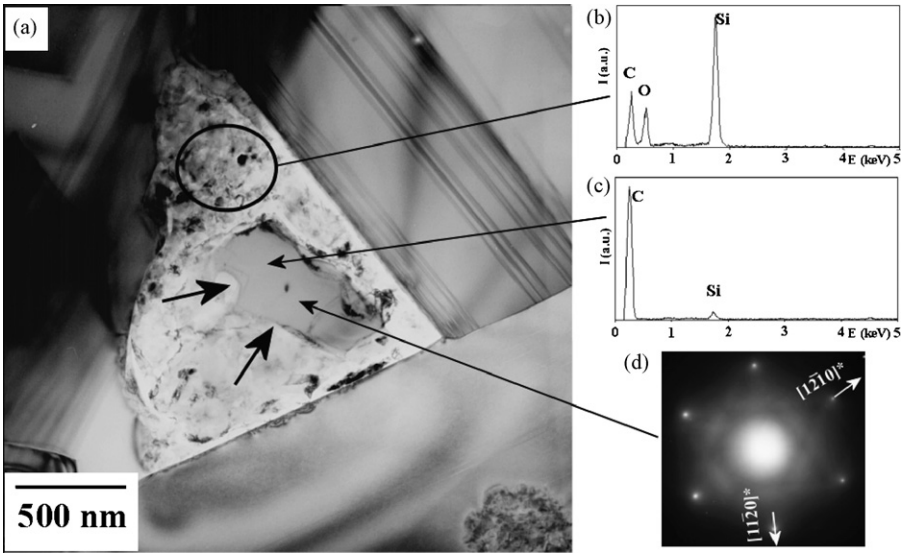

Fig. 8. TEM micrograph of a reaction site (see also encircled areas in Fig. 7). Overview showing the B_4C crystal surrounded by a composite glassy phase (a). It shows corrosion gulfs which attest that a dissolution process takes place. Energy dispersive spectrometry (EDS) analysis of the outer composite interphase (b). EDS analysis of the B_4C grain (c). [0 0 0$\bar{1}$] SAED pattern of the B_4C compound (d).

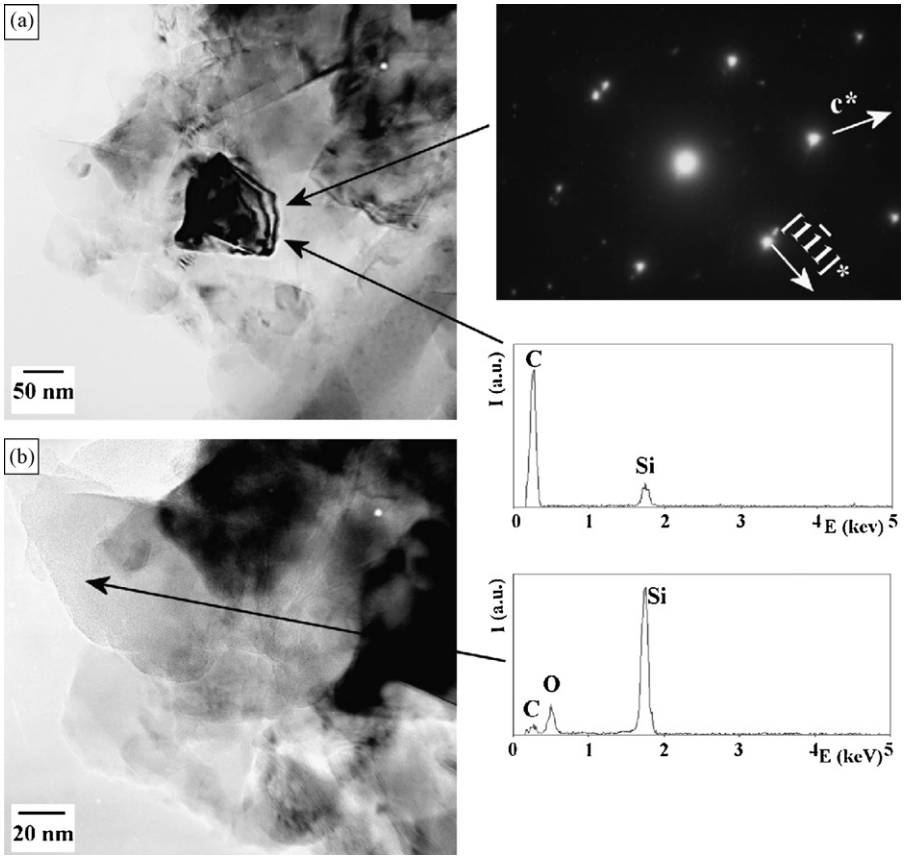

Fig. 9. TEM observations of the composite interphase shown in Fig. 8. Conventional imaging of a diamond nanocrystal (a) and its associated SAED pattern and EDXS analysis. The diamond nanocrystals are embedded within an amorphous silica rich phase (b).

consequently, unambiguously permits to conclude that diamond or more probably carbon-like diamond resulted from the SPS treatment.

The spherical intragranular inclusions (Fig. 10) are also formed by the same reactional product, *i.e.* carbon-like diamond crystals (Fig. 10b) embedded within the silicate phase (Fig. 10c). In this case, relicts of B_4C crystals are never observed.

Finally, the comparison of FTIR patterns for both the starting silicon carbide powder and the sintered SB4C sample (Fig. 11) reveals the presence of additional Si–O ($\approx$1100 cm^{-1}) and O–Si–O ($\approx$470 cm^{-1}) bands[23] in the case of SPS treated samples. These results suggest that the oxidation of SiC grains occurs during the heat treatment.

4. Discussion

4.1. SPS treatment of pure SiC

This study has shown that Spark Plasma Sintering had a great effect on the kinetic of the densification of "pure" α-silicon carbide. Indeed, to reach fully dense SiC-based materials (without sintering additives) by using conventional pressurized techniques such as hot-pressing or hot isostatic pressing, it is well known that severe experimental conditions are required:[8,24] high sintering temperature ($T \geq 2100\,^{\circ}C$) and high soaking time ($t \geq 30$ min).

These drastic treatments usually lead to the thermal decomposition of the SiC compound and may involve the coalescence of grains and pores.[11] Conversely, the SPS treatment by reducing the holding time to 5 min and by lowering the sintering temperature to 1950 °C allows minimizing grain growth (Fig. 6a) and, consequently, provides equiaxed microstructure. These SPS conditions permit also to achieve high relative densities for SiC specimens (*i.e.* 97.5%) without sintering activators.

These results should be due to the characteristics of the SPS heating treatment such as self-heat generation by microscopic electric discharge between particles, this activation leading to high speed mass and heat transfer.[25,26] More particularly, the rapid densification could be correlated to mechanisms with faster kinetics, such as surface diffusion, diffusion through the melt, or time-independent process such as plastic deformation.[27–29] So, the melting could occur only on the particle surface thanks to electron discharge which easily generates localized heating on the grains.

4.2. Effect of boron additions on the SPS behaviour of SiC-based specimens

The form under which the same amount of carbon and boron was added to the starting SiC powder plays a key role in the sintering process involved during the treatment. From all the results

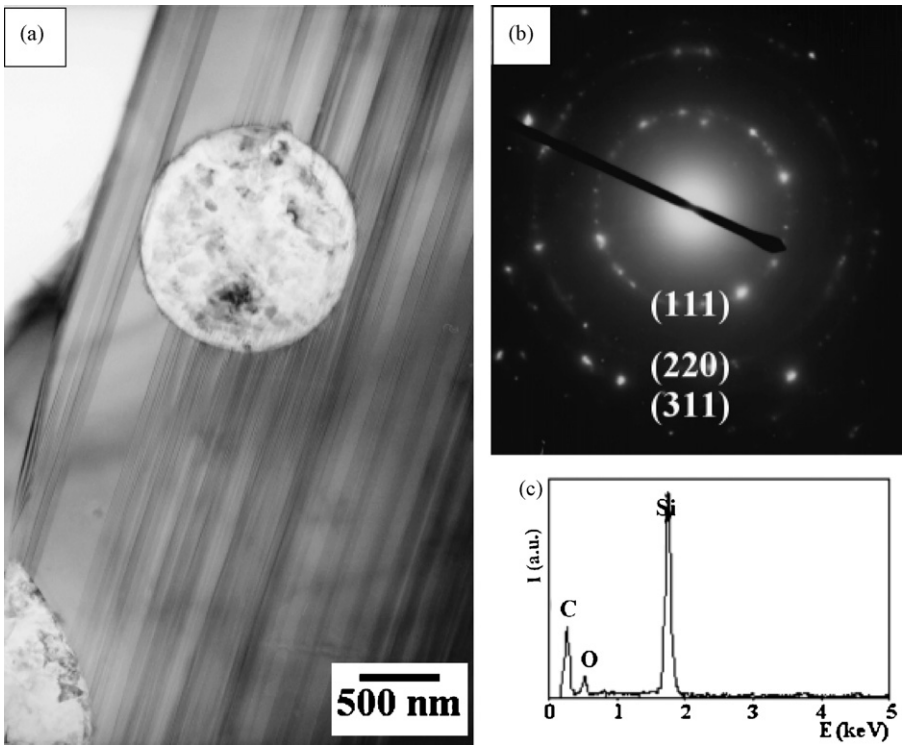

Fig. 10. TEM observation of an intragranular inclusion (see also arrows in Fig. 7) (a). The SAED pattern (b) and the EDS analysis (c) obtained on the overall area of the composite interphase show the presence of diamond nanocrystals embedded within a silica rich phase.

of sintering attempts and microstructural characterizations, the role of boron additions could be elucidated.

In SB4C samples, the B_4C crystals are shown to be dissoluted at the contact of a silicate phase, giving rise to a liquid phase sintering process. FTIR investigations and EDXS analyses revealed that this phase would result from the reaction between the silica-based phase due to the native oxidation of silicon carbide grains and the boron carbide crystals introduced as sintering aids. The native oxidation of SiC is a well-known phenomenon which results from the sorption of water molecules at room temperature.[30] The SPS treatment of SB4C samples would favour the reaction between the silica film surrounding the SiC grains and the B_4C compound. The presence of thin jagged reaction fronts around boron carbide grains attest of the dissolution mechanism of B_4C into the liquid silica-based phase (Fig. 8), finally providing a borosilicate glass after cooling. Therefore, the results obtained from the microstructural characterization of SB4C sintered samples permit to explain the role of a secondary fusible phase on the microstructure evolution during SPS. At the forming temperature, the borosilicate phase was partly a viscous liquid, which presumably controlled grain boundary migration. When the temperature increases, its viscosity drastically decreases, promoting the mobility of grain boundaries by favouring atomic diffusion within the liquid phase. It is reasonable to assume that the grain growth kinetic by dissolution/reprecipitation mechanism should be enhanced for some crystallographic orientations which probably correspond to the surfaces of lowest energy for the SiC phase. Thanks to the high motion of the grain boundary, some pockets of liquid phase were entrapped within the grains leading to spherical intragranular inclusions.

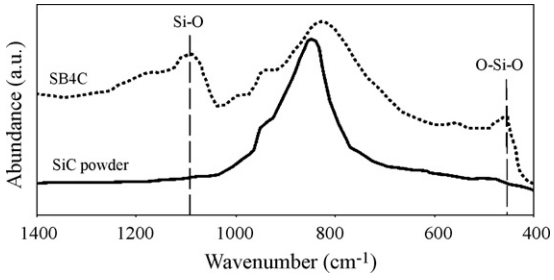

Fig. 11. Infrared spectra of pure silicon carbide before SPS treatment (continuous line: SiC powder) and of SB4C samples (SiC powder plus boron carbide) sintered by SPS at 1950 °C for 5 min under 100 MPa (discontinuous line).

For the SBC samples, TEM investigations revealed that the formation of secondary phase is precluded, as no continuous thin film of interphase or glassy pockets at triple junctions were evidenced. This result is in fair agreement with a previous study[31] which showed that no distinct amorphous film can be found by HREM imaging of such interfaces. However, the interface seemed to be highly perturbed and thanks to spatially resolved electron energy-loss spectroscopy, these authors have shown that one monolayer of boron segregates at the SiC boundary. According to these authors,[32] the main effect of boron doping on the densification of silicon carbide should rely on the enhancement of the grain boundary diffusion. In fact, they indicated that most of the added boron would segregate at the grain boundary because of its low solid solubility at the sintering temperature (*e.g.* ≤ 0.1 wt% at $T = 2200$ °C).[33–34] Conversely, Elder and Krstic [35] suggested that the additive boron is dissolved in

the β-SiC matrix, forming a solid solution that enhanced lattice diffusion through the increase of carbon vacancies ratio in SiC. This latter phenomenon could explain the enhancement of the mass transfer during sintering. The same interpretation was retained by Datta et al.[36] for a α-SiC powder.

In the present study, despite the fact that the sintering additives are present in much higher amount (3.1 wt%), *i.e.* ten times higher than those reported in ref.[32], no interphase was detected. This result would suggest that the sintering aids effect could rather rely on formation of solid solutions with the SiC compound, even if their location could be restricted to the interface vicinity. In this hypothesis, the role of free boron addition on the densification activation (Fig. 4) could be explained by the creation of further silicon and carbon vacancies in the lattice of the SiC compound following Eqs. (1) and (2):

$$B_4C \xrightarrow{SiC} 4B'''_{Si} + C^{\times} + 3V^{\bullet\bullet\bullet\bullet}_{C} \quad (1)$$

$$SiB_4 \xrightarrow{SiC} 4B^{\bullet\bullet\bullet}_{C} + Si^{\times} + 3V'''_{Si} \quad (2)$$

Finally, in these SBC samples, the free carbon addings present in well-distributed manner would reduce the native silica film on the surface of SiC grains during the sintering[37] by the overall reaction:

$$SiO_{2(s)} + 3C_{(s)} \rightarrow SiC_{(s)} + 2CO_{(g)} \quad (3)$$

5. Conclusion and perspectives

This study confirms the favourable role of boron additions on the sintering of SiC by Spark Plasma Sintering processes.

The most efficient SPS treatment to reach fully dense SiC-based materials consists in both introducing free carbon and free boron and maintaining a 100 MPa pressure at 1950 °C for 5 min. Free carbon should favour the reduction of silica covering the surfaces of SiC grains whereas free boron additions could improve the densification kinetic by enhancing the formation of further point defects in the α-SiC lattice. It is thus possible to conclude that the volume diffusion certainly intervains as one of the mechanism that largely operates during the sintering of SiC. This does not preclude the possible influence of competitive process such as grain boundary diffusion.

In the case of boron carbide additions, the occurrence of a borosilicate liquid phase during the SPS treatment results from the reaction of dissolution of B_4C in contact with the silica based phase coming from the native oxidation of the starting SiC powder. This secondary liquid phase promotes an abnormal grain growth leading to a slight non-densifying effect. The next studies should refine the mechanism of boron carbide dissolution and the main properties of the glassy phase obtained during the sintering treatment.

Acknowledgements

This work was financially supported by ALCAN Company and especially by the Research Centre of Voreppe (CRV). The authors should like to express their appreciation for the technical assistance of Dr. Claude Estournes who is responsible for the French SPS platform (called PNF[2] and financially supported by CNRS). The authors are also grateful to Mr. Etienne Laborde, Mr. Bernard Soulestin and Dr. Daniel Tétard for their technical assistance.

References

[1]. Skybakmoen, E., Gudbransen, H. and Stoen, L. I., Chemical resistance of sidelining materials based on SiC and carbon in cryolithic melts—a laboratory study. *Light Metals*, 1999, 215–222.

[2]. Skybakmoen, E., Gudbransen, H. and Stoen, L. I., Evaluation of chemical resistance–oxidation of Si_3N_4-SiC sidelining materials used in Al electrolysis cells. In *Proceedings of Unified Technical Conference on Refractories 3*, 2001, pp. 1330–1339.

[3]. Nadeau, J. S., Very high pressure hot pressing of silicon carbide. *Am. Ceram. Soc. Bull.*, 1973, **52**, 170–174.

[4]. Sakai, T., Watanabe, H. and Aikawa, T., Effects of carbon on phase transformation of β-SiC with Al_2O_3. *J. Mater. Sci. Lett.*, 1987, **6**, 865–866.

[5]. Omori, M. and Takei, H., Preparation of pressureless-sintered β-SiC with Al_2O_3. *J. Mater. Sci.*, 1988, **23**, 3744–3749.

[6]. Antonova, N. D., Kalinina, A. A. and Kudryatsev, V. I., Preparation and some properties of materials based on silicon with boron and aluminium additions. *Sov. Powder Metal. Metal Ceram.*, 1962, **6**, 444–450.

[7]. Prochazka, S., The role of boron and carbon in the sintering of silicon carbide, in: Popper P., editor. *Special Ceramics*, *vol. 6*. British Ceramic Research Association, England; 1975, p. 171–81.

[8]. Bind, J. M. and Biggers, J. V., Hot-pressing of silicon carbide with 1% boron carbide addition. *J. Am. Ceram. Soc.*, 1975, **58**, 304–306.

[9]. Magnani, G., Beltrami, G., Minoccari, G. L. and Pilotti, L., Pressureless sintering and properties of α-SiC-B_4C composite. *J. Eur. Ceram. Soc.*, 2001, **21**, 633–638.

[10]. Stobierski, L. and Gubernat, A., Sintering of silicon carbide. Effect of boron. *Ceram. Int.*, 2003, **29**, 355–361.

[11]. Stobierski, L. and Gubernat, A., Sintering of silicon carbide. Effect of carbon. *Ceram. Int.*, 2003, **29**, 287–292.

[12]. Ermer, E., Wieslaw, P. and Ludoslaw, S., Influence of sintering activators on structure of silicon carbide. *Solid State Ionics*, 2001, **141-142**, 523–528.

[13]. Yamamoto, T., Kitaura, H., Kodera, Y., Ishii, T., Ohyanagi, M. and Munir, Z. A., Consolidation of nanostructured β-SiC by Spark Plasma Sintering. *J. Am. Ceram. Soc.*, 2004, **87**, 1436–1441.

[14]. Gao, L., Wang, H. Z., Hong, J. S., Miyamoto, H., Miyamoto, K., Nishikawa, Y. and Torre, S. D. D. L., Mechanical and microstructure of nano-SiC-Al_2O_3 composites densified by Spark Plasma Sintering. *J. Eur. Ceram. Soc.*, 1999, **19**, 609–613.

[15]. Takeuchi, T., Tabuchi, M., Kageyama, H. and Suyama, Y., Preparation of dense $BaTiO_3$ ceramics with submicrometer grains by spark plasma sintering. *J. Am. Ceram. Soc.*, 1999, **82**, 939–943.

[16]. Gao, L., Shen, Z. J., Miyamoto, H. and Nygren, M., Superfast densification of oxide/oxide ceramic composites. *J. Am. Ceram. Soc.*, 1999, **82**, 1061–1063.

[17]. Liu, Q., Huang, Z., Shen, Z. and Nygren, M., Improved densification of Al_2O_3 and SiC based ceramic composites by spark plasma sintering, advances and matrix composites VI. *Ceram. Trans.*, 2001, **124**, 127–137.

[18]. Zhou, Y., Hirao, K., Toriyama, M. and Tanaka, H., Very rapid densification of nanometer silicon carbide powder by pulse electric current sintering. *J. Am. Ceram. Soc.*, 2000, **83**, 654–656.

[19]. Shen, Z., Johnsson, M., Zhao, Z. and Nygren, M., Spark Plasma Sintering of alumina. *J. Am. Ceram. Soc.*, 2002, **85**, 1921–1927.

[20]. TOPAS version 3, Brüker-AXS, Karlsruhe (Germany), (1999-2000).

[21]. Ortiz, A. L., Sanchez-Bajo, F., Padture, N. P., Cumbrera, F. L. and Guibertean, F., Quantitative polytype-composition analyses using X-ray diffraction: a critical comparison between the polymorphic and the Rietveld Methods. *J. Eur. Ceram. Soc.*, 2001, **21**, 1237–1248.

[22]. ICSD (Inorganic Crystal Structure Database), FIZ-NIST, Version 2007-1.

[23]. Abdelmounîm, E., PhD thesis, University of Limoges, 1994 (in French).

[24]. Dutta, S., Densification and properties of α-silicon carbide. *J. Am. Ceram. Soc.*, 1985, **8**, C269–C270.

[25]. Chen, W., Anselmi-Tamburini, U., Garay, J. E., Groza, J. R. and Munir, Z. A., Fundamental investigations on the spark plasma sintering/synthesis process: I. Effect of dc pulsing on reactivity. *Mater. Sci. Eng. A*, 2005, **394**, 132–138.

[26]. Anselmi-Tamburini, U., Gennari, S., Garay, J. E. and Munir, Z. A., Fundamental investigations on the spark plasma sintering/synthesis process: II. Modeling of current and temperature distributions. *Mater. Sci. Eng. A*, 2005, **394**, 139–148.

[27]. Chaim, R., Densification mechanisms in spark plasma sintering of nanocrystalline ceramics. *Mater. Sci. Eng. A*, 2007, **443**, 25–32.

[28]. Tamari, N., Tanaka, T., Tanaka, K., Kondoh, I., Kawahara, M. and Tokita, M., Effect of Spark Plasma Sintering on densification and mechanical properties of silicon carbide. *J. Ceram. Soc. Jap.*, 1995, **103**, 740–742.

[29]. Gao, L. and Miyamoto, H., Spark Plasma Sintering technology. *J. Inorg. Mater.*, 1997, **12**, 129–133.

[30]. Médout-Marère, V., El Ghzaoui, A., Charnay, C., Douillard, J. M., Chauveteau, G. and Partyka, S., Surface heterogeneity of passively oxidized silicon carbide particles: hydrophobic-hydrophilic partition. *J. Colloid Interface Sci.*, 2000, **223**, 205–214.

[31]. Gu, H., Shinoda, Y. and Wakai, F., Detection of boron segregation to grain boundaries in silicon carbide by spatially resolved by electron energy-loss spectrometry. *J. Am. Ceram. Soc.*, 1999, **82**, 469–472.

[32]. Shinoda, Y., Yoshida, M., Akatsu, T. and Wakai, F., Effect of amount of boron doping on compression deformation of fine-grained silicon carbide at elevated. *J. Am. Ceram. Soc.*, 2004, **87**, 1525–1529.

[33]. Tajima, Y. and Kingery, W. D., Solid Solubility of aluminum and boron in silicon carbide. *J. Am. Ceram. Soc.*, 1982, **65**, C27–C29.

[34]. Linnarsson, M. K., Zimmermann, U., Wong-Leung, J., Schöner, A., Janson, M. S., Jagadish, C. and Svensson, B. G., Solubility limits of dopants in 4H-SiC. *Appl. Surf. Sci.*, 2003, **203-204**, 427–432.

[35]. Elder, P. and Krstic, V. D., Effect of surface area on densification of β-SiC powders in the presence of B and c. *Br. Ceram. Trans. J.*, 1992, **91**, 67–71.

[36]. Datta, M. S., Bandyopadhyay, A. K. and Chaudhuri, B., Sintering of nanocrystalline α-silicon carbide by doping with boron carbide. *Bull. Mater. Sci.*, 2002, **25**, 181–189.

[37]. 37, W. J. and Clegg, Role of carbon in the sintering of boron-doped silicon carbide. *J. Am. Ceram. Soc.*, 2000, **83**, 1039–1043.